arXiv:astro-ph/9911501v1 29 Nov 1999

Cosmic Flows 99: Conference Summary

Avishai Dekel

Racah Institute of Physics, The Hebrew University, Jerusalem 91904, Israel

Abstract. I address the following issues: All bulk velocity measurements (but one) are consistent with our standard gravitational instability theory. New accurate data and reconstruction methods allow high-resolution dynamical analysis nearby, revealing Virgo, Ursa Major and Fornax as attractors. Large peculiar-velocity surveys enable robust reconstruction of the dynamical fields on the Great-Attractor scale. A decomposition of the velocity field into its local and tidal components indicates the presence of big perturbations further away. Cluster velocities start exploring very large scales, revealing Coma, Shapely and other mass enhancements, and constraining a possible local Hubble bubble. Supernovae type Ia (SNIa) are very promising for cosmic flow analysis. Peculiar velocities do provide unique valuable constraints on cosmological parameters, e.g., $0.3 < \Omega_{\rm m} < 1$ (95% confidence) independent of biasing. Jointly with other data they can confine other parameters such as Ω_Λ, h, σ_8, n, and the biasing. Nontrivial features of the biasing scheme can explain much of the span of estimates for β. Quantitative error analysis is essential in our maturing field; every method ought to be calibrated with suitable mock catalogs, that are offered as benchmarks.

1. Introduction

This is not a comprehensive review of the conference, but rather a collection of concluding remarks on some of the central issues which I wish to highlight. The distinctive feature of this conference was the exposure of several new observational surveys of peculiar velocities, listed in Table 1. These data enable dynamical studies in three zones: our $30\,h^{-1}$Mpc local neighborhood at high-resolution, within $\sim 60\,h^{-1}$Mpc with $\sim 10\,h^{-1}$Mpc smoothing, and out to $\sim 120\,h^{-1}$Mpc at low-resolution. I use some of the analysis tools developed by my colleagues and myself, including POTENT, Wiener Filter (WF), decomposition and likelihood analysis, to illustrate some of the potential of these data. I then address the implications to cosmology and galaxy formation, and my views of how further progress is ought to be made.

The outline is as follows: §2. addresses bulk velocities. §3. discusses high-resolution analysis in the local neighborhood. §4. reviews the robust analysis in the Great Attractor vicinity. §5. proposes a decomposition of the velocity field into divergent and tidal components. §6. demonstrates the

potential of dynamical analysis on very large scales. §7. addressed the constraints on cosmological parameters. §8. evaluates the effect of nontrivial biasing on the range of estimates for β. §9. stresses the importance of error analysis via mock catalogs. §10. summarizes my main points.

Table 1: Peculiar Velocity Data

Catalog	Dist. Ind.	Err %	Objects	Num. ga/cl	Rad. h^{-1}Mpc	Reference
SBF	SBF	8	E/ga	300	30(40)	Blakeslee *et al.*, tv
PT	TF	18	S/ga	500	30(40)	Pierce, Tully, tv
ENEAR	FP	20	E/ga,cl	1900	40(70)	Wegner *et al.*, tv
M3	TF,FP	18	S,E/ga,cl	3400	50(80)	Willick *et al.* 97a
SFI	TF	18	S/ga	1650	50(70)	Haynes *et al.* 98a,b
Shellflow	TF	18	S/ga	300	40-75	Courteau *et al.*, tv
SNIa	SN	8	S	44	50(200)	Riess, tv
SCI+II	TF	18	S/cl	1300/76	95(200)	Dale & Giovanelli, tv
SMAC	FP	20	E/cl	700/56	65(140)	Smith *et al.*, tv
LP10K	TF	18	S/cl	170/15	90-135	Willick, tv
BCG	$L_{\rm m}$-α	18	E/cl	120	85(150)	Lauer & Postman 94
EFAR	FP	20	E/cl	450/85	60-150	Colless *et al.*, tv

2. Bulk Velocity

The simplest quantity extracted from a peculiar velocity sample is the bulk velocity V, in a sphere (or a shell) about the Local Group (LG). The measurements are sometimes referred to as either proving "convergence" to the cosmic frame within a given radius, or as posing a challenge to the large-scale isotropy of the universe. I would like to stress that the interpretation of a bulk velocity is meaningful only in the context of a specific theoretical model, and is a quantitative issue. In fact, large-scale isotropy does not require "convergence" on any finite scale. Our models predict, quite robustly, a relatively weak descent of amplitude with scale, and the large cosmic variance due to the finite, sparse and nonuniform sampling can accommodate a large range of results.

I therefore point first, in Fig. 1, to the theoretical prediction of a ΛCDM model for the simplest statistic: the bulk-flow amplitude in a top-hat sphere. The solid line is the rms value, obtained by integrating over the power spectrum times the square of the Fourier Transform of the top-hat window. The dashed lines represent 90% cosmic scatter in the Maxwellian distribution of V, when only one random sphere is sampled. This model (flat, with $\Omega_{\rm m} = 0.35$, $n = 1$, $h = 0.65$), has $\sigma_8\Omega_{\rm m}^{0.5} = 0.51$, consistent with the constraints from cluster abundance (Eke, Cole & Frenk 1996). In fact, any model from the CDM family that is normalized in a similar way predicts bulk velocities in the same ball-park, so the theoretical curves should be regarded as representative of our "standard" models. Note the gradual descent and the large scatter: the velocity could almost vanish inside $50\,h^{-1}$Mpc, or be as high as $400\,{\rm km\,s^{-1}}$ near $100\,h^{-1}$Mpc, without violating standard cosmology.

A bulk velocity can be computed by fitting a 3D model of constant velocity to the observed radial peculiar velocities. Each datum contributes to the fit,

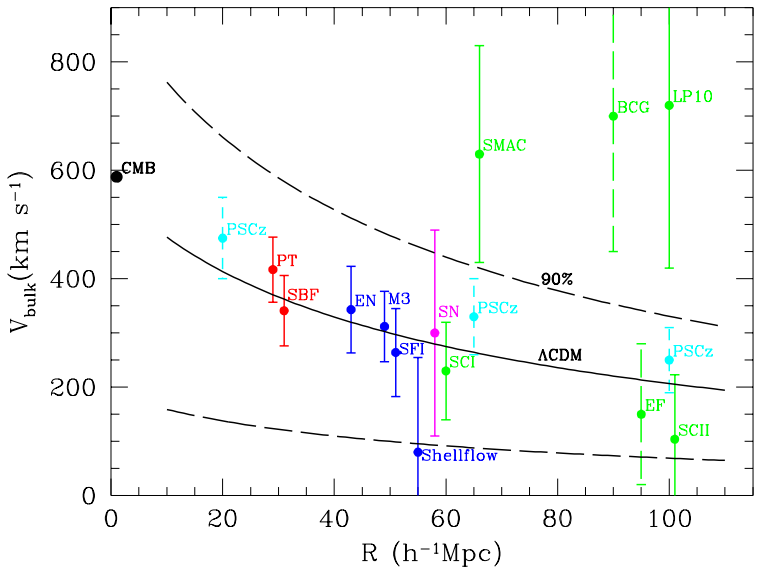

Figure 1. Amplitude of CMB bulk velocity in top-hat spheres about the LG, in comparison with theory. The curves are the predicted rms and cosmic scatter for a ΛCDM model. The measurements, based on the data listed in Table 1, are crudely translated to a top-hat bulk velocity. The errorbars are random only. All the non-zero vectors (except BCG) point to $(l, b) = (280, 0) \pm 30°$. Shown as well are the LG dipole velocity and linear estimates from the PSCz redshift survey for $\beta = 0.7$.

usually weighted by the inverse square of the relative distance error, added in quadrature to a constant velocity dispersion. Thus, the result corresponds to a nonuniform window in space, which is typically biased towards small radii and is very specific to the sample. A proper comparison with theory should take into account the sampling window and the associated cosmic scatter (Kaiser 1988; Watkins & Feldman 1995). However, a semi-quantitative impression can be obtained by a crude comparison in the "theory plane", for which one can approximate a top-hat window by equal-volume weighting at the expense of larger random errors. A full POTENT analysis is a more accurate way of mimicking uniform weighting.

The results are put together in a crude way in Fig. 1, displaying the amplitudes of the bulk velocities in the CMB frame, as if they all represent top-hat bulk velocities. The amplitudes can be compared because the directions of all the nonzero vectors are remarkably similar: with the exception of BCG, they all lie in the 30° vicinity of $(l, b) = (280, 0)$. Some of the error-bars are based on a careful error analysis using mock catalogs, while others are crude estimates. In most cases they represent random errors only and underestimate the systematic biases. The bulk velocities were de-biased by subtracting in quadrature the errors in each component.

Also shown in Fig. 1 is the velocity of the LG as deduced from the CMB dipole, and the velocities predicted from the IRAS PSCz redshift survey using

linear theory, with $\beta_{\rm IRAS} = 0.7$, the best-fit to the CMB dipole (Saunders *et al.*, this volume, hereafter tv).

M3, SFI and Shellflow are dominated by Tully-Fisher (TF) spirals inside $R \lesssim 50\,h^{-1}$Mpc. The M3 result refers to the VM2 calibration (Dekel *et al.* 1999) and is a bit lower than the original M3 result. The M3 and SFI results were obtained via a uniform POTENT reconstruction and error analysis. Inside $R \lesssim 50\,h^{-1}$Mpc they generally agree, while at larger radii the bulk velocity in SFI drops faster than in M3. This difference may be related to a difference in matching the zero points of the TF relations between North and South in the two catalogs, but one should admit that these two samples are not large enough for a reliable estimate of V beyond $50\,h^{-1}$Mpc, where, for one thing, the Malmquist-bias corrections are quite uncertain. The new Shellflow result seems to favor a low value, but it is for a shell outside the main body of M3 and SFI, and the large error due to the relatively small number of galaxies makes it consistent with the model, and with both M3 and SFI, at the $\sim 1\sigma$ level. However, the Shellflow data will enable a revised calibration of M3 and SFI, which can significantly reduce the uncertainties. The preliminary report from the ENEAR survey of Fundamental-Plane (FP) velocities (Wegner *et al.*, tv) agrees well with M3 and SFI.

In our local $30\,h^{-1}$Mpc vicinity, we have computed the bulk flows via a minimum χ^2 fit with volume weights for the two independent new surveys: the accurate SBF measurements of 300 ellipticals (Tonry *et al.*, tv), and TF measurements of 500 spirals (Pierce, Tully, tv). A dispersion of $\sim 300\,{\rm km\,s^{-1}}$ is assumed in the fit, to make $\chi^2 \simeq$ d.o.f. One can see that all the results within $50\,h^{-1}$Mpc are remarkably consistent with our theoretical expectations and with each other.

On larger scales we have several new results based on clusters of galaxies: SMAC and EFAR of FP ellipticals, and LP10K and SCI+II based on TF spirals. The EFAR sample is an exception because it covers limited areas of sky, largely perpendicular to the direction of the bulk flow. The fact that all these results are consistent with the same bulk-flow direction is very comforting in view of the worries raised earlier by the BCG result.

The amplitudes, on the other hand, show large scatter. The results are as reported by the observing teams, with an effective top-hat radius crudely assigned. The main point is that no one single measurement is more than $\sim 2\sigma$ away from the model prediction, even in the simplified presentation of in Fig. 1. This is confirmed by a more accurate analysis which takes into account the systematic errors due to sampling together with the random errors and cosmic variance (Hudson, tv; Hoffman, tv). A model with a steeper drop in the power spectrum on the "blue" side of the peak, like CHDM, gives a somewhat higher amplitude and therefore a better fit to SMAC and LP10K.

Hudson demonstrates further that the bulk velocity vectors as measured in all of these large-scale surveys (except BCG) are in fact consistent with each other at the 95% CL. Take for example the "high" LP10K value compared to the "low" SCII value. We note that the individual peculiar velocities of the 7 clusters common to these samples are consistent within the errors, and that the 15 SCII clusters that lie within the LP10K shell have a nominal bulk velocity of $\sim$400, closer to the LP10K result. I therefore do not see the need or justification

for Willick (tv) to discard his own result; it is high, but consistent with the model and the other data given the expected (big) errors.

As pointed out by Strauss (tv), there is no clear understanding yet of the source of the discrepant BCG result, and we are therefore eagerly waiting for the upcoming, follow-up, larger BCG survey for a possible resolution of this mystery.

The bulk velocity of SNIa is computed by us, volume weighted and de-biased, from the 16 SNe inside $60\,h^{-1}$Mpc (out of the sample of 44 inside $300\,h^{-1}$Mpc, Riess, tv). Even slightly higher values are obtained (with no volume weights) inside $\sim 100\,h^{-1}$Mpc. The SN result still carries a large error because of the small number of objects in the current sample, but the accurate distances and the unlimited sampling potential promise that this distance indicator will eventually become very valuable in reducing the uncertainties on large scales.

Despite the apparent scatter on large scales, and the disputes over the bulk velocity being small or large, we see no significant discrepancies between the bulk velocity data and models, and thus the bulk flow measurements do not introduce a problem for homogeneous cosmology. Even though there seems to be a slight preference for CHDM-like models, the bulk velocity is clearly not the tool for distinguishing between the variants of our standard picture. On the other hand, the fact that the model predictions for the bulk velocity are robust (especially once forced to roughly obey the normalization constraints from other data) allows us to use the observed amplitude of $\sim 300\,\mathrm{km\,s^{-1}}$ bulk velocity on scales $\lesssim 100\,h^{-1}$Mpc, in comparison with the observed $\delta T/T \sim 10^{-5}$ in the CMB, as a unique probe of the fluctuation growth rate. This provides the most convincing confirmation for our basic hypothesis that structure has evolved by gravitational instability (see Bertschinger, Gorski & Dekel 1989; Zaroubi *et al.* 1997a).

3. Local Neighborhood

The new SBF peculiar velocities (Tonry, Dressler, tv; Blakeslee *et al.*, tv), in which the distance of each galaxy is estimated with unprecedented accuracy and Malmquist biases are small, allow a high-resolution study of the dynamics in our local cosmological neighborhood, within $30\,h^{-1}$Mpc of the LG. Fig. 2 demonstrates the potential of this data via a high-resolution map of the mass-density field as recovered by a Wiener-Filter. This method (Zaroubi, Hoffman & Dekel 1999; originally Kaiser & Stebbins 1991) provides the most likely mean density field, given the noisy data and an assumed model for the power spectrum (in this case a tilted $\Omega = 1$ CDM which best fits the M3 data). The method assumes that both the density fluctuations and the errors are Gaussian, and it uses linear gravity. Note that the WF induces variable smoothing as a function of the local noise; it allows a high-resolution analysis nearby, where the data is of high quality, with an effective smoothing of nearly G4 (a Gaussian window of $4\,h^{-1}$Mpc), compared to ∼G10 with the M3 and SFI data on larger scales.

While showing (on the left) the near side of the known Great Attractor (GA), the map reveals for the first time fine dynamical entities nearby. The counterparts of these structures in the galaxy distribution are clearly seen in the

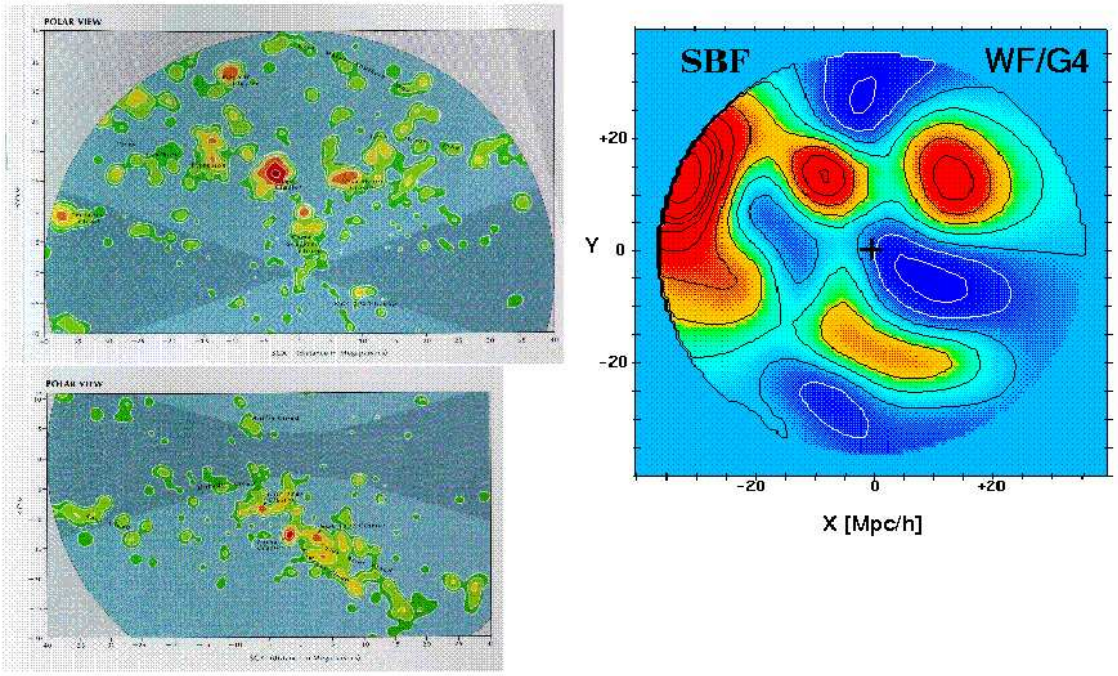

Figure 2. The local Supergalactic Plane at high resolution. *Right:* Reconstructed mass density field using Wiener Filter of $4\,h^{-1}$Mpc from SBF peculiar velocities. *Left:* Galaxy distribution from the Nearby Galaxies Atlas (distances in h_{75}^{-1}Mpc). Local clusters such as Virgo (middle), Ursa Major (right) and Fornax (bottom), are recovered as attractors.

corresponding maps from the Nearby Galaxies Atlas (Tully & Fisher 1987, plates 15 and 19). For example, the Virgo and Ursa Major clusters, branching out from the GA along Y$\sim 15\,h^{-1}$Mpc all the way to X~ 30, and the Fornax complex, stretching in the south Galactic hemisphere (Y< 0) out to X~ 20. The general similarity between the galaxy clusters and the underlying mass attractors is encouraging. A quantitative comparison would allow a study of the non-trivial biasing relation between galaxies and dark matter in the local vicinity, on scales smaller than addressed so far.

A sample of $\sim$ 500 TF peculiar velocities within $30\,h^{-1}$Mpc is being completed by Pierce, Tully and coworkers, and the ENEAR survey will add ellipticals in this region. Together with the accurate SBF data, they present a new opportunity for high-resolution dynamical analysis of the local neighborhood. For example, these new data call for a revisited VELMOD analysis of comparison between peculiar velocities and a whole-sky redshift survey (Willick *et al.* 1997b; Willick & Strauss 1999). It should be borne in mind that a proper high-resolution analysis must treat nonlinear effects in a reliable way, which must be tested using proper mock catalogs (§9.).

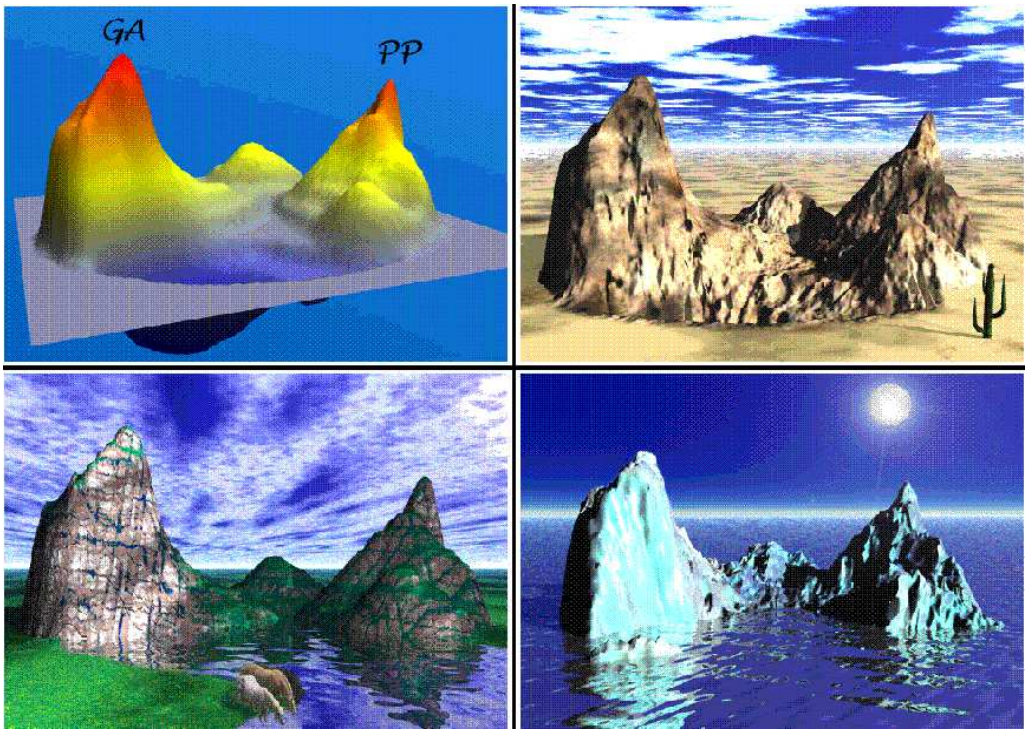

Figure 3. Top-left: mass-density distribution in the Supergalactic plane out to $70\,h^{-1}$Mpc, by POTENT G12 from M3 peculiar velocities, featuring the GA, PP, and the big void in between. The height represents density. The other panels are artist concepts (courtesy of Ofer Dekel). The icebergs in the bottom-right reflect the "coldness" of the flows...

4. Great Attractor and Perseus Pisces

The M3 and SFI datasets, soon to be cross-calibrated with the whole-sky Shellflow, and then to be complemented by ENEAR, provide a rich body of peculiar velocity data for a quantitative analysis of the dynamical fields on intermediate-large scales. By applying methods like POTENT to these data we obtain reliable reconstructions with uniform G12 smoothing out to $\sim 60\,h^{-1}$Mpc (at least in several directions). Fig. 3 shows the G12 density field in the Supergalactic plane as extracted by POTENT from the M3 peculiar velocities. The dominant structures are the Great Attractor (GA, left), Perseus-Pisces (PP, right), and Coma (back), with the big void stretching in between.

Fig. 4 shows Supergalactic density maps as reconstructed from different datasets and by different methods. The VM2 calibration of M3, which has been tailored to maximize the agreement of M3 with the IRAS 1.2Jy redshift survey, hardly makes a difference to the density map (while it does reduce the bulk flow somewhat). The appearance of the GA is quite similar in M3 and SFI, while PP in SFI is lower and located further away, with the big void between the LG and PP deeper and more extended (and thus pointing to a larger value

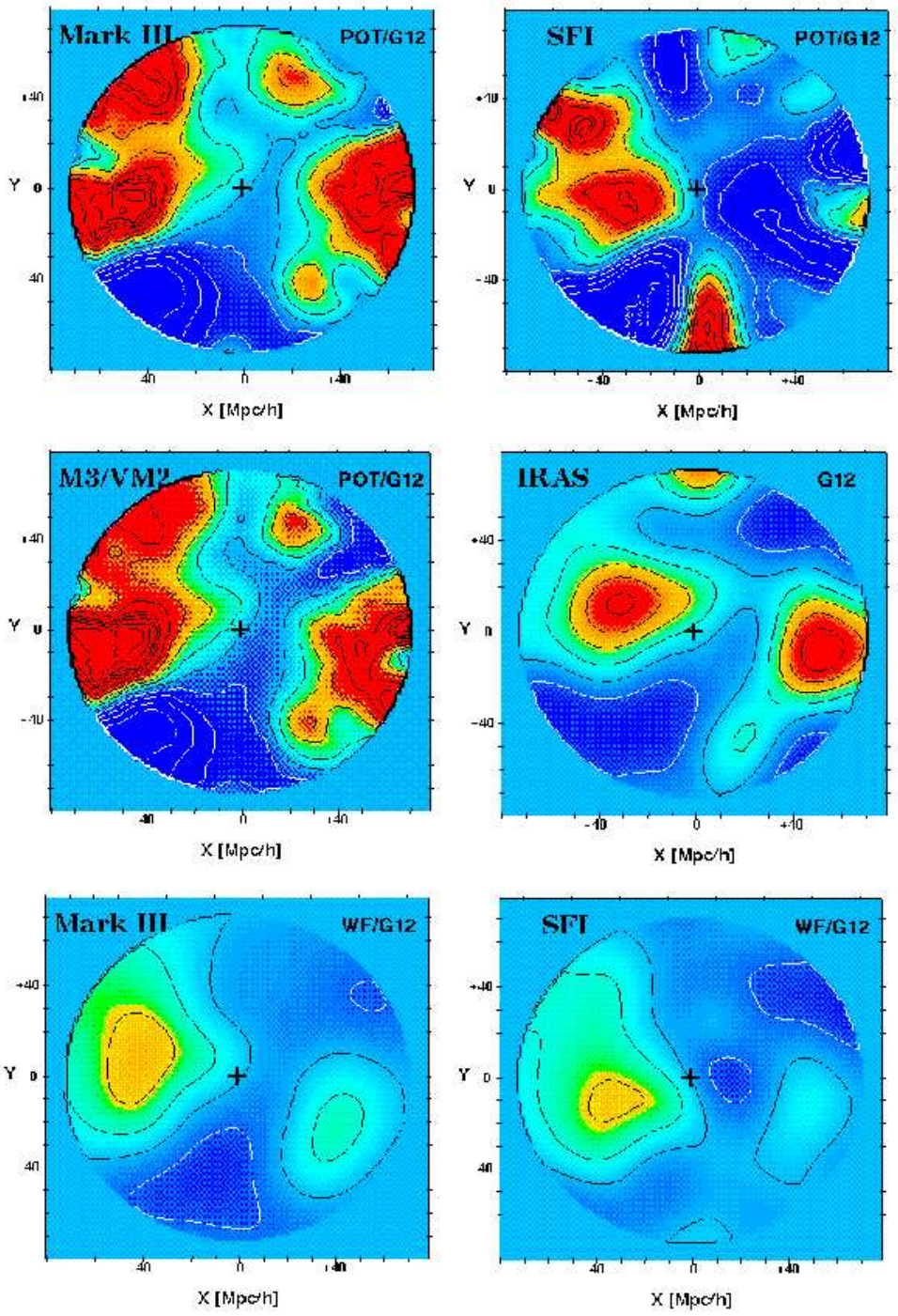

Figure 4. Density maps of the Supergalactic plane out to $70\,h^{-1}$Mpc. The G12 POTENT reconstructions from M3 (original and VM2 calibration, top- and middle-left) and SFI peculiar velocities (top-right) can be compared to each other and to the IRAS galaxy distribution (middle-right). The WF maps (bottom) highlight the robust features.

of $\Omega_{\rm m}$, §7.). There is a general similarity between the dynamical mass-density maps (for M3 more than SFI) and the IRAS 1.2Jy galaxy-density map, allowing a reconstruction of the local biasing field (§8.). The WF mean field density contrast at a given location is, by construction, correlated with the quality of the data there. The WF maps thus demonstrate that the M3 and SFI densities are similar in the regions of high-quality data, such as the GA region, and they highlight the robust large-scale dynamical features in our neighborhood. The M3 and SFI results differ mostly in their bulk velocities in shells near $50-60\,h^{-1}$Mpc — a problem that Shellflow may help resolving.

5. Decomposition: Local and Tidal Components

There has been a lot of discussion over the years about which object is responsible for what velocity. In general, this discussion is conceptually confused because the acceleration at a point is the integral of the density fluctuations over all of space and it cannot be uniquely assigned to any specific source.

Nevertheless, given a specific volume, one can uniquely decompose the velocity at any point into two well-defined components: a "divergent" and a "tidal" component, due to the density fluctuations within the volume and outside it, respectively. A demonstration of such a decomposition is shown in Fig. 5, for the mean velocity field recovered using a WF from the M3 peculiar velocities, with respect to a sphere of radius $60\,h^{-1}$Mpc about the LG. The WF velocity field is first translated into a density field via linear theory, $\delta \propto -\boldsymbol{\nabla}\cdot\boldsymbol{v}$, and then the divergent velocity field is reconstructed by integrating the inverse of this Poisson equation inside the sphere of $60\,h^{-1}$Mpc. The tidal field is obtained by subtracting the divergent component from the total velocity.

The divergent component shows the main features of convergence and divergence within the volume, associated with the GA, PP, and the voids in between. The CMB velocity of the LG is about half divergent, namely due to GA, PP and such, and half tidal, due to mass fluctuations external to the $60\,h^{-1}$Mpc sphere. There is no significant bulk velocity in the divergent component inside that sphere (although there could be one, e.g., if there was only a single dominant off-center attractor in this sphere); The bulk velocity inside the sphere of $60\,h^{-1}$Mpc is all tidal, due to external fluctuations. When this bulk velocity is subtracted from the tidal component, one recovers the shear field, dominated by the quadrupole and higher moments. The major eigenvector of the shear tensor lies roughly along the line connecting the LG with the Shapley supercluster. A fit of a simplified toy model made of a single point-mass attractor to the tidal component yields a mass excess of $\approx 4\times10^{17}h^{-1}\Omega^{0.4}M_\odot$ at a distance of $\approx 175\,h^{-1}$Mpc in the direction of Shapley.

This analysis thus allows us to extract information from the velocities in a given volume about the mass distribution outside this volume, and it can be applied to different datasets and different volumes. For example, when applied to the WF (or POTENT) velocities from the SFI data inside $60\,h^{-1}$Mpc, the tidal bulk velocity turns out smaller than in the M3 case, but the residual shear field is very similar, indicating a similar quadrupole and external sources. When applied to the SBF data within $30\,h^{-1}$Mpc, the decomposition yields similarly

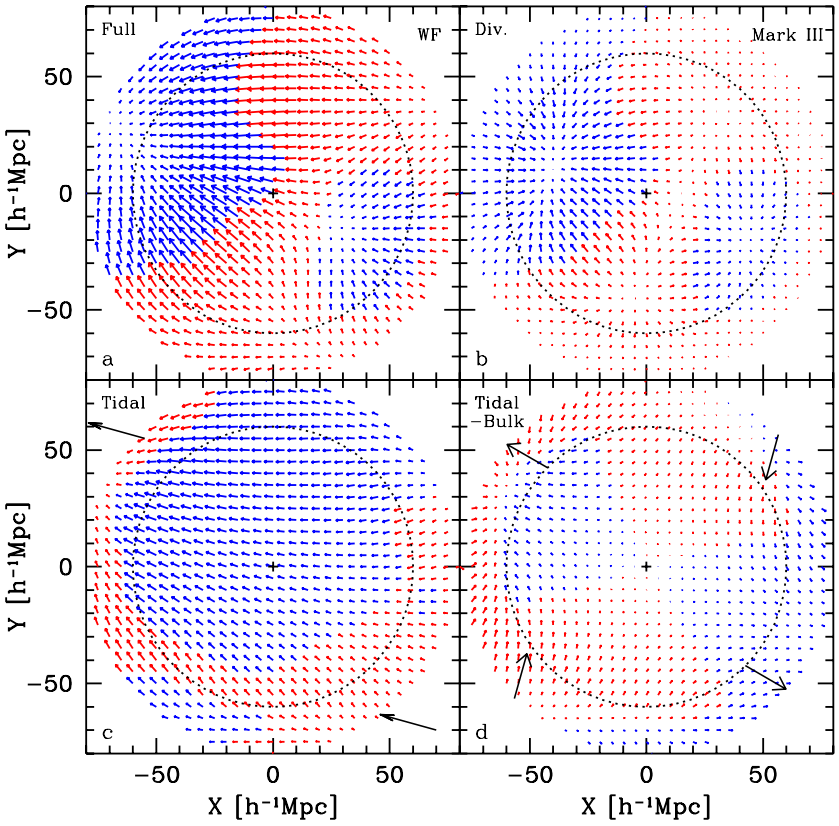

Figure 5. A decomposition of the M3 WF velocity field in the Supergalactic plane (a) into its "divergent" component, due to the mass fluctuations within $60\,h^{-1}$Mpc (b), and its "tidal" component, due to the external mass distribution (c). The residual after subtracting the bulk velocity from the tidal component is the shear, including quadrupole and higher moments in the tidal field (d). Velocities and distances are measured in $100\,\mathrm{km\,s^{-1}}$ or h^{-1}Mpc. In the upper panels, the color marks the sign of $\nabla\cdot\boldsymbol{v}$, and thus hints to the local density contrast. In (c), blue refers to velocities that are aligned ($\pm30^\circ$) with the tidal bulk velocity. In (d), the color corresponds to the sign of the radial velocity, highlighting the quadrupole.

that the bulk velocity is dominated by the tidal field, and the major axis of the shear tensor lies roughly along the line connecting PP, LG and GA.

6. Very Large Scales

The new data of peculiar velocities for clusters of galaxies on large scales allow dynamical reconstruction beyond just the bulk velocity. As a demonstration, Fig. 6 shows G20 POTENT maps extracted from a combination of the SMAC, LP10K, and SN data out to $120\,h^{-1}$Mpc. Beyond the familiar structures of GA and PP that dominate the inner $\sim60\,h^{-1}$Mpc, one can see the Coma structure at

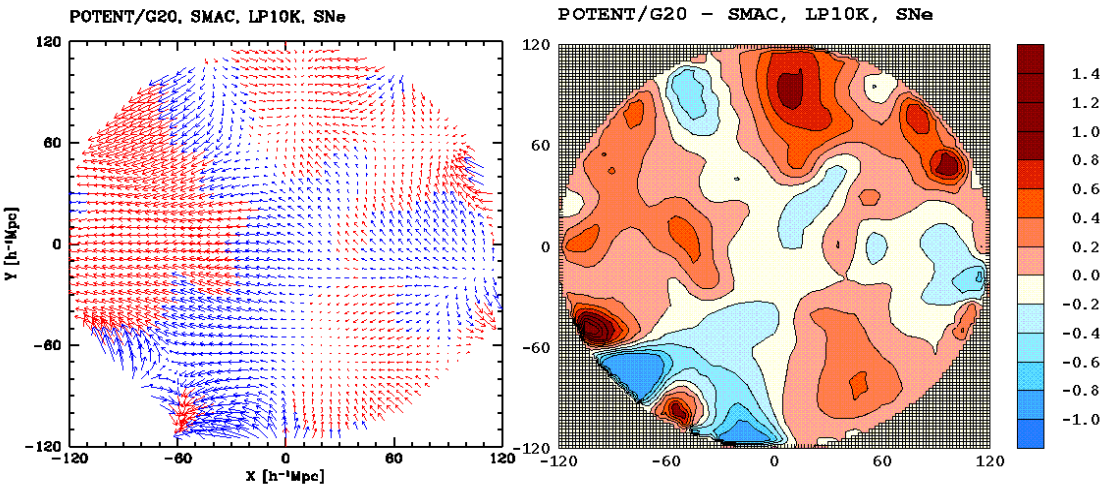

Figure 6. G20 POTENT reconstruction on very large scales from peculiar velocities of clusters and SNe. The near sides of the big mass enhancements associated with the Shapley and Horologium superclusters show up on the left, and with Coma at the top.

Y$\sim 50 - 100\,h^{-1}$Mpc, and the near sides of the Shapely (Y>0) and Horologium (Y<0) overdensities behind the GA, at X$\sim -100\,h^{-1}$Mpc and beyond. The earlier hints from the tidal component of the velocities at smaller distances (Fig. 5) are now beginning to be confirmed by the local derivatives of the peculiar velocities directly measured at large distances.

Another example for a large-scale study is the monopole analysis, which could constrain a local Hubble Bubble (Zehavi *et al.* 1997; Dale & Giovanelli, tv; Fruchter, tv) and thus modify the local estimates of h and $\Omega_{\rm m}$ (§7.). Peculiar velocities of many objects both inside the void and far outside it are necessary for a reliable result. With more and more data at large distances, the monopole deviations from the universal Hubble flow could be determined with increasing accuracy, because the error $\delta H = \delta v/r$ is independent of distance (as $\delta v \propto r$).

I think that the greatest potential for future studies of local cosmic flows lies in big surveys of SN Ia (Riess, tv). They provide a distance indicator of only 5-10% error which can be observed out to hundreds of megaparsecs and is, in principle, of unlimited sampling density, limited in practice only by the patience and dedication of the observers.

7. Cosmological Parameters

I share the discontent expressed by Strauss (tv) and others from the fact that the results from cosmic flows have been unjustifiably underrated by many in the community. This has a lot to do with bad PR on our side, where in many cases we tend to stress marginal apparent discrepancies between different results and take for granted the robust valuable findings.

An important feature of peculiar velocity data is that it allow us to addresses directly the dynamics of the total (cold) mass distribution, and thus bypass

the difficulties introduced by density biasing of the luminous galaxies, which are unavoidable in the analysis of redshift surveys. For example, the spatial velocity variations provide direct constraints on the value of the cosmological density parameter $\Omega_{\rm m}$. This makes them valuable even when the errors are not yet as small and under control as they could be, given that the available complementary data all involve additional parameters such as σ_8, Ω_Λ, or biasing parameters, and they all have their own appreciable errors. The results obtained on intermediate scales directly from M3 and SFI constrain $\Omega_{\rm m}$ at the $\pm 2\sigma$ level to the range 0.3-1.0 (Primack, tv; based on Nusser & Dekel 1993; Dekel & Rees 1993; Bernardeau *et al.* 1995; and yet unpublished results from the newer data).

Allowing the power spectrum to be of the CDM type, the maximum-likelihood estimate of $\Omega_{\rm m}$ is 0.5 ± 0.1 (Zaroubi *et al.* 1997b; Freudling *et al.* 1999). A similar analysis with more free parameters can constrain additional parameters that affect the power spectrum, such as the large-scale power index n, or the normalization parameter σ_8.

The results from cosmic flows provide valuable orthogonal constraints to complementary data. For example, combined with the constraints from the global geometry of space-time based on high-redshift supernovae type Ia, which is roughly $0.8\Omega_{\rm m} - 0.6\Omega_\Lambda = -0.2 \pm 0.1$ (Riess *et al.* 1998; Perlmutter *et al.* 1999), the velocity constraints on $\Omega_{\rm m}$ confine the value of Ω_Λ to 0.8 ± 0.3 (Zehavi & Dekel 1999). Jointly with available CMB constraints as well, one can obtain simultaneous constraints on three parameters, such as $\Omega_{\rm m}$, σ_8 and h (Zehavi & Dekel, tv), still without appealing to biasing parameters. The addition of constraints from the abundance of clusters (Eke, Cole & Frenk 1996), or from gravitational lensing, should allow us to confine these dynamical parameters with even higher accuracy.

We heard evidence for the "coldness" of the local flow (Lake, tv; Van de Weygaert & Hoffman, tv; Klypin, tv), which left us still wondering whether it is really in conflict with standard models (Strauss, tv). I dare to report on a very preliminary result of a likelihood analysis based on M3 and SFI (extending Zehavi & Dekel, tv), which seems to favor a power spectrum that drops sharply at $k \gtrsim k_{\rm peak}$. Such a power spectrum could be obtained, for example, with a high faction of baryonic or hot dark matter. A similar, independent hint comes from the SMAC data (Hudson *et al.*, tv). This would add to the uncertainty of the results obtained under the assumption of ΛCDM.

When a redshift survey is involved, the unknown biasing relation between galaxies and mass introduces another source of uncertainty, which should not be ignored. One should treat biasing properly before $\Omega_{\rm m}$ can be extracted from the range of estimates of parameters like β (§8.).

Many different clever ideas of how to estimate cosmological parameters from peculiar velocities can be thought of. Some turn out to be more discriminatory and less biased than others. A given idea can turn into a viable method, whose results should be considered seriously, only after the method has been tested and calibrated using proper mock catalogs, and a detailed error analysis is provided (§9.). If this attitude is adopted by all practitioners, the field will regain the respectability it deserves in evaluating the cosmological parameters.

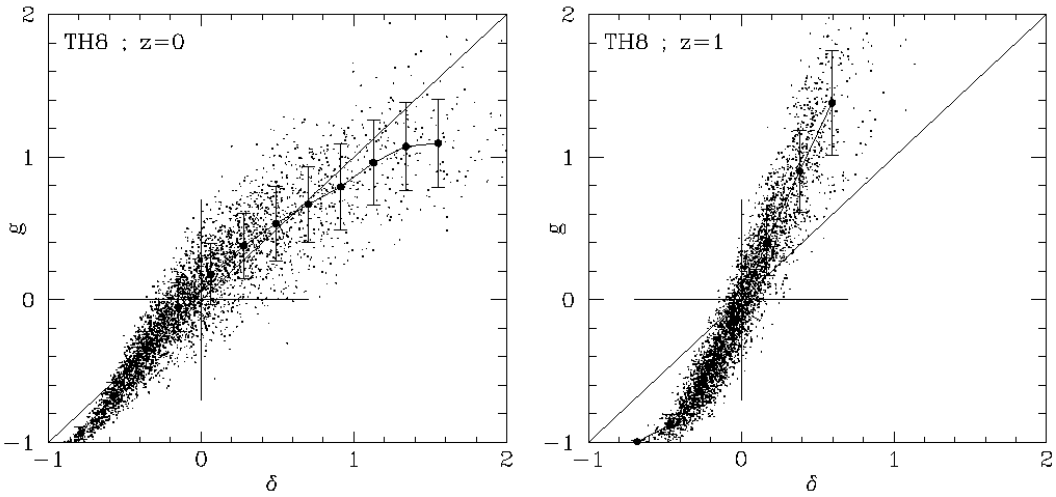

Figure 7. Biasing of galactic halos ($>2\times10^{12}\mathrm{M}_\odot$) versus mass in an N-body simulation, demonstrating nonlinearity and stochasticity. The smoothed (top-hat $8\,h^{-1}$Mpc) density fluctuation fields are plotted at grid points. The conditional mean and scatter are marked (bars). *Left:* at $z=0$, when $\sigma_8=0.6$, showing characteristic nonlinear behavior in underdense regions. *Right:* at $z=1$, when $\sigma_8=0.3$, demonstrating strong time evolution.

8. Biasing

Understanding the biasing relation between galaxies and mass is crucial for the purpose of translating measurements of bias-contaminated quantities such as β (vaguely defined as $\Omega^{0.6}/b$) into accurate estimates of Ω. On the other hand, the biasing can provide hints for the complicated physical processes involved in galaxy formation.

The linear deterministic relation between the density fluctuations of galaxies and mass, $\delta_{\rm g}(\boldsymbol{x}) = b\,\delta(\boldsymbol{x})$, has no theoretical basis and is not self-consistent. Indeed, the analytic analysis of halo biasing (Mo & White 1996) predicts that the biasing is non-linear, $b=b(\delta)$. Then, the biasing at any other smoothing scale must obey a different $b(\delta)$ and be non-deterministic, i.e., it involves scale-dependence and scatter. In addition to shot noise, an inevitable source of scatter are hidden variables affecting the efficiency of galaxy formation beyond its dependence on δ, which are yet to be studied in detail (e.g., Blanton *et al.* 1998). Fig. 7 demonstrates some of the nontrivial qualitative features of halo biasing in N-body simulations. The nonlinear shape of $b(\delta)$ at $\delta<0$ is robust, while at $\delta>0$ it varies with mass, time and scale (see also Frenk, tv; Sheth, tv).

In order to properly incorporate the biasing in the analysis of cosmic flows, one needs an appropriate formalism that quantifies non-trivial biasing. For example, in the formalism of Dekel & Lahav (1999), the linear and deterministic relation at a given scale and time is replaced by the conditional distribution $P(\delta_{\rm g}|\delta)$. The mean nonlinear biasing is characterized by the conditional mean $\langle\delta_{\rm g}|\delta\rangle \equiv b(\delta)\,\delta$, and the scatter by the conditional variance $\sigma^2_{\rm b}(\delta)$. To second order, the biasing is then defined by 3 parameters: the slope $\hat{b}$ of the regression

of δ_g on δ (replacing b), a non-linearity parameter $\tilde{b}/\hat{b}$, and a scatter parameter $\sigma_b/\hat{b}$. The ratio of variances b^2_{var} and the correlation coefficient r mix these fundamental parameters. In the case shown in Fig. 7 at $z = 0$, the overall non-linearity is $\tilde{b}^2/\hat{b}^2 = 1.08$, and the scatter is $\sigma^2_b/\hat{b}^2 = 0.15$. These effects lead to differences of order 20-30% among the various measures of β. An additional contribution to the span of β estimates may have to do with the biasing dependences on scale and on galaxy properties. These are deduced from simulations such as the one shown in Fig. 8 (e.g., Somerville *et al.* 1999), and can be measured from large redshift surveys with type identification, such as SDSS. Together, these nontrivial biasing features could explain much of the observational range, $\beta_{IRAS} = 0.4 - 1.0$ (Strauss, tv, Table 2). Any outliers are suspicious of underestimated errors, and should be re-examined using proper mock catalogs (§9.).

9. Error Analysis

The research field of cosmic flows, which started in the eighties with semi-qualitative analyses, has developed into a mature, quantitative phase in which the errors ought to be evaluated in detail. This will allow us to understand the range of estimates for parameters like β and Ω_m. Measurements based on new methods or data which are not accompanied by a detailed error analysis are not very useful at this point (though such results are still being presented at times).

An appropriate tool for error analysis is an ensemble of Monte Carlo mock catalogs, in which both the nonlinear gravitational dynamics and the galaxy formation process are simulated properly, and then galaxies are sampled and measured in a way that mimics the observational procedure. Such mock catalogs allow an evaluation of both random and systematic errors.

The development of the POTENT method (Dekel *et al.* 1999; Kolatt, tv) is an example. The recovery algorithm and the associated methods for measuring cosmological parameters have been calibrated based on mock catalogs by Kolatt *et al.* (1996). A key feature of these simulations was the effort to mimic the actual structure in our local neighborhood, generating the initial conditions using constrained realizations based on the density of galaxies in the IRAS 1.2Jy redshift survey. Such simulations allow for correlations between the errors and the underlying density field. The main limitations of these mock catalogs were the unsatisfactory treatment of nonlinear effects due to limited resolution in the simulations, the simplified way of identifying galaxies, and the fact that the simulations were initially restricted to an $\Omega_m = 1$ standard CDM cosmology. It is now time for a new generation of mock catalogs that will overcome these limitations.

New mock catalogs of this sort are becoming available, based on the GIF simulations (Eldar *et al.* 1999). Constrained realizations (based on IRAS 1.2Jy) serve as initial conditions that were evolved forward in time using a high-resolution parallel tree code, assuming either τCDM ($\Omega_m = 1$) or ΛCDM ($\Omega_m = 0.3$), both with power spectra that allow a simultaneous fit to COBE normalization and the observed cluster abundance. Particle positions and velocities were stored at 50 logarithmically spaced time-steps in order for

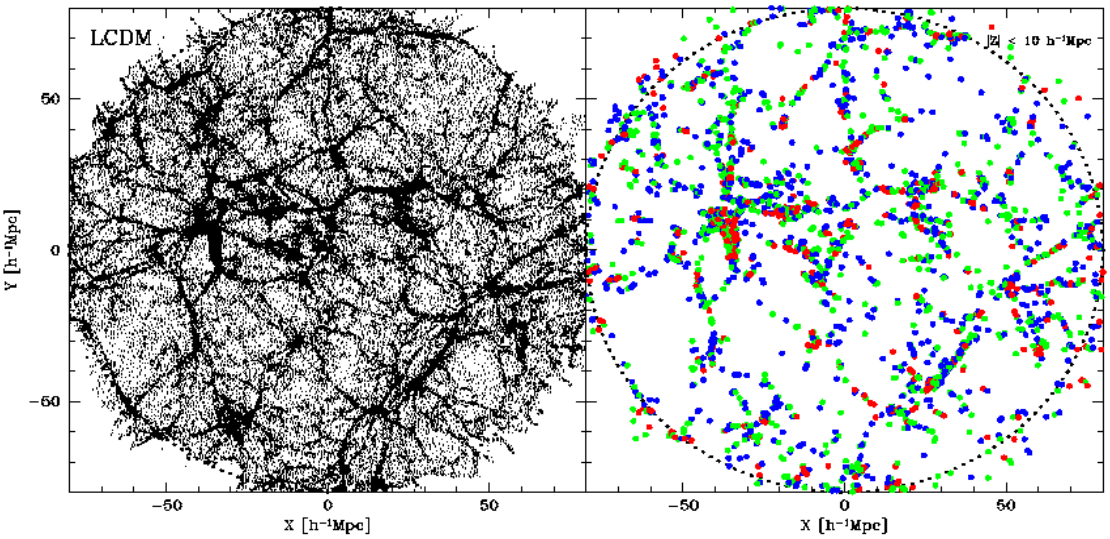

Figure 8. Constrained simulations in the Supergalactic Plane. The large-scale structure is constrained to fit the density in the IRAS 1.2Jy redshift survey, while the small-scale fluctuations are drawn from a ΛCDM power spectrum. *Left:* Dark Matter, showing the GA (top-left), PP (bottom-right), etc. *Right:* Modeled galaxies in the same slice, color coded by B-V, demonstrating how red, early-type galaxies reside in clusters. This is the basis for mock catalogs that serve as benchmarks for methods.

different recipes of galaxy formation to be implemented *post hoc* in considerable detail. The physical processes include shock heating (and possibly radiative heating) of the pre-galactic gas, radiative cooling, star-formation, hydrodynamic (and possibly radiative) feedback from supernovae, and enrichment with heavy elements. Fig. 8 shows a slice from the ΛCDM constrained simulation, comparing the dark-matter distribution with the galaxy distribution.

Given the relevant properties for each of the galaxies, such as magnitude and internal velocity, one can "observe" a set of Monte-Carlo mock catalogs following the selection criteria and specifications of each of the observed catalogs (e.g., Diaferio *et al.* 1999). By applying one's algorithm to these mock catalogs, for which the "true" underlying dynamics is known, one can quantify the random and systematic errors in detail. These simulations and mock catalogs will soon be made available as standard benchmarks for reconstruction methods. Designer mock catalogs for specific new datasets can be made to order.

10. Conclusion

My main points are as follows:

• The observed amplitudes of bulk velocity out to $\sim 100\,h^{-1}$Mpc (with the marginal exception of the current BCG result) are consistent with our standard family of cosmological models. Full "convergence" is not really required on any scale. The main lesson from the bulk velocity is its general consistency with

the gravitational growth rate of perturbations starting from the fluctuations at recombination as measured in the CMB.

• The SBF and other data provide an opportunity for high-resolution dynamical analysis of the local neighborhood out to $30\,h^{-1}$Mpc. Virgo, Ursa Major and Fornax show up as local attractors, and can help us model the biasing relation on small scales, provided that nonlinear effects are treated properly.

• The dynamical structure of the GA is robust in the M3 and SFI datasets. The Shellflow data should improve the cross-calibration of North and South in the M3 and SFI data, which, together with other data, ought to allow an accurate evaluation of the bulk velocity out to $\sim 70\,h^{-1}$Mpc.

• A decomposition of the velocity field into divergent and tidal components allow us to tell that a significant part of the bulk velocity inside $60\,h^{-1}$Mpc is due to external density fluctuations, and that the shear field points at the Shapely concentration as a massive attractor.

• The extended cluster and SN velocities enable dynamical analysis beyond just bulk flow out to $120\,h^{-1}$Mpc, confirming the mass enhancements associated with Coma, Shapely and Horologium. The available data provide marginal evidence for a local Hubble Bubble, that should become less ambiguous with more SN data.

• Supernovae type Ia seem to be the most promising tool for cosmic flow analysis. The SN hunters are thus encouraged to pursue large surveys at low redshifts.

• Peculiar velocities do provide interesting constraints on cosmological parameters. For example, they confine $\Omega_{\rm m}$ to the range 0.3-1.0 at 95% confidence, independent of biasing or other data, solely based on the assumption of Gaussian initial fluctuations. Combined with other data, this constraint is translated to constraints on other parameters, such at Ω_Λ, σ_8, h, etc.

• Galaxy biasing is an obstacle for translating a measured value of β into an estimate of $\Omega_{\rm m}$. Nontrivial features of the biasing scheme, including nonlinearity, stochasticity, scale dependence and type dependence, as predicted by models and simulations, can explain much of the span of estimates for β.

• Quantitative error analysis is essential in order to complete the transition of large-scale dynamics into a mature field. Every method has to be calibrated with appropriate mock catalogs, in which nonlinear dynamics and galaxy formation are simulated properly. Such mock catalogs are being produced and offered as benchmarks.

Where next? The field of cosmic flows enjoyed several influential conferences, starting in Hawaii, Rio and the Vatican in 1985-1987, then Paris in 1993, and now Victoria in 1999. Projecting ahead, we should look forward to meeting again with exciting new results around 2005. This is provided that somebody energetic like Stephane Courteau takes charge in organizing such a conference.

Acknowledgments. I am especially indebted to Ami Eldar, the current guardian of POTENT, for the computations and maps. I am grateful to all my collaborators, many of which have participated in this conference. Our work has been partially supported by the US-Israel Binational Science Foundation (95-00330, 98-00217), by the Israel Science Foundation (950/95, 546/98), and by NASA (ATP NAG 5-301). I believe I represent all the conference participants in thanking Stephane Courteau for organizing this very successful conference.

References

Bernardeau, F., Juszkiewicz, R., Dekel, A., & Bouchet, F.R. 1995, MNRAS, 274, 20

Bertschinger, E., Gorski, K., & Dekel, A. 1990, Nature, 345, 507

Dale, D.A., Giovanelli, R. , Haynes, M.P., Campusano, L.E., Hardy, E., & Borgani, S. 1999, ApJL, 510, L11 (SCI+II)

Blanton, M., Cen, R., Ostriker, J.P., & Strauss, M.A. 1999, ApJ, 522, 590

Dekel, A., Burstein, D., & White, S.D.M. 1997, in Critical Dialogues in Cosmology, ed. N. Turok (World Scientific), p. 175

Dekel, A., Eldar, A., Kolatt, T., Yahil, A., Willick, J.A., Faber, S.M., Corteau, S., & Burstein, D. 1999, ApJ, 522, 1 (POTENT)

Dekel, A., & Lahav, O. 1999, ApJ, 520, 24

Dekel, A., & Rees, M.J. 1993, ApJL, 422, L1

Diaferio, A., Kauffmann, G., Colberg, J.M., & White, S.D.M. 1999, MNRAS, 307, 537

Eldar, A., Dekel, A., Lemson, G., Mathis, H., Kauffmann, G., & White, S.D.M. 1999, in preparation

Eke, V.R., Cole, S., & Frenk, C.S. 1996, MNRAS, 282, 263

Freudling, W., Zehavi, I., daCosta, L.N., Dekel, A., Eldar, A., Giovanelli, R., Haynes, M.P., Salzer, J.J., Wagner, G., & Zaroubi, S. 1999, ApJ, 523, 1

Haynes, M.P., Giovanelli, R., Salzer, J.J., Wegner, G., Freudling, W., da Costa, L.N., Herter, T., & Vogt, N.P. 1998a, AJ, 117, 1668 (SFI)

Haynes, M.P., Giovanelli, R., Chamaraux, P., da Costa, L.N., Freudling, W., Salzer, J.J., & Wegner, G. 1998b, AJ, 117, 2039 (SFI)

Hudson, M.J., Smith, R.J., Lucey, J.R., Schlegel, D.J. & Davies, R.L. 1999, ApJL, 512, L79 (SMAC)

Kaiser, N. 1988, MNRAS, 231, 149

Kaiser, N. & Stebbins, A. 1991, in Large Scale Structure and Peculiar Motions in the Universe, eds. D.W. Latham & L.N. da Costa (ASP Conference Series), p. 111

Kolatt, T., Dekel, A., Ganon, G., & Willick, J. 1996, ApJ, 458, 419

Lauer, T.R. & Postman, M. 1994, ApJ, 425, 418 (BCG)

Mo, H.J. & White, S.D.M. 1996, MNRAS, 283, 154

Nusser, A., & Dekel, A. 1993, ApJ, 405, 437

Perlmutter, S. *et al.* 1999, ApJ517, 565

Riess, A.G., Davis, M., Baker, J., & Kirshner, R.P., 1997, ApJL, 488, L1 (SNIa)

Riess, A.G. *et al.* 1998, AJ, 116, 1009

Somerville, R.S., Lemson, G., Sigad, Y., Dekel, A., Kauffmann, G., & White, S.D.M. 1999, MNRAS, submitted

Tully, R.B., & Fisher, J.R. 1987, Nearby Galaxies Atlas (Cambridge University Press)

Watkins, R. & Feldman, H.A. 1995, ApJL, 453, L73

Willick, J.A. 1999, ApJ, 516, 47 (LP10K)

Willick, J.A., Courteau, S., Faber, S.M., Burstein, D., Dekel, A., & Strauss, M.A. 1997a, ApJS, 109, 333 (M3)

Willick, J.A., Strauss, M.A., Dekel, A., & Kolatt, T. 1997b, ApJ, 486, 629 (VELMOD)

Zehavi, I., & Dekel, A. 1999, Nature, 401, 252

Zehavi, I., Riess, A.G., Kirshner, R.P., & Dekel, A. 1998, ApJ, 503, 483

Zaroubi, S., Sugiyama, N., Silk, J., Hoffman, Y., & Dekel, A. 1997a, ApJ, 490, 473

Zaroubi, S., Zehavi, I., Dekel, A., Hoffman, Y. & Kolatt, T. 1997b, ApJ, 486, 21

Zaroubi, S., Hoffman, Y., & Dekel, A. 1999, ApJ, 520, 413

Zehavi, I., Riess, A.G., Kirshner, R.P., & Dekel, A. 1998, ApJ, 503, 483.

To appear in "Cosmic Flows: Towards an Understanding of Large-Scale Structure", eds S. Courteau, M.A. Strauss, & J.A. Willick, ASP Conf. Series